ELSEVIER

Metal complexation of chitosan and its glutaraldehyde cross-linked derivative

Athena Webster, Merrill D. Halling and David M. Grant*

University of Utah, Chemistry Department, Salt Lake City, UT 84112, USA

Abstract—The physicochemical characterization of metal complexed with chitosan (CS) and its glutaraldehyde cross-linked derivative (CSGA) was investigated. Seven metal ions from chromium through zinc of the first row of the transition metals were selected for complexation. Structural features pertinent to where and how metals bind into both polymers are our main interest. Studies using solid-state NMR spectroscopy and XRPD (X-ray powder diffraction) supported by ESR spectroscopy, ICP-OES (inductively couple plasma-optical emission spectroscopy) and far-FTIR spectroscopy for metal interaction with nitrogen sites at C-2 of the metal–polymer complexes were performed. Theoretical calculations of the metal–polymer ratio, the approximate charges on nitrogen for both amine and imino-linker, and the proton affinity between an alcohol group from the polymer and an amino/imino group are reported. A helical coiled chitosan model and a 2C1L (two-chitosans with one linker) model are proposed here. The metal uptake mechanism for both polymers is concluded to be absorption within the polymers, rather than adsorption on the polymer surface.
© 2007 Elsevier Ltd. All rights reserved.

Keywords: Chitosan; Glutaraldehyde cross-linked chitosan; Metal interaction; Amine; Imine; Schiff base; Metal interaction; Metal–polymer complexes

1. Introduction

Chitosan (CS) is a β-(1→4)-linked biopolymer of 2-amino-2-deoxy-D-glucose (glucosamine)[1–4] repeating units,[5,6] which is the N-deacetylated derivative of chitin and selectively absorbs transition metal ions.[3,4,7–9] Many literature references have focused on the effect of pH and ionic strength[3,9,10] in the control of metal uptake by CS.[3,11,12] The synthesis and modification of these polymers are not the main theme in this study, but rather the physical interactions of metal–polymer complexes and an investigation of the metal–nitrogen interactions in CS and its glutaraldehyde cross-linked derivatives.

Highly porous and hydrated cross-linked CS beads have been designed to increase metal ion chelation and metal adsorption capability in the past.[13–15] Modifica-

tions to increase the number of binding sites and/or binding surfaces of polyglycans have been made both by changing the secondary amine at C-2 and by cross-linking the polyglycans with small chemicals. Cross-linking CS with biomass/biopolymers like alginate,[13,16] polymers like polyvinyl alcohol (PVA),[14] chelators like ethylenediamine tetraacetic acid (EDTA),[17] or fixatives like glutaraldehyde (GA)[18] creates a three-dimensional network within the biopolymer and increases the internal surface area for metal adsorption.[10] Glutaraldehyde has been commonly used in many cross-linking procedures.[10] The aldehyde groups are reported as highly active, readily forming Schiff bases with amino groups. Increase in structural and chemical stability of these cross-linked derivatives contributes to the resistance and endurance of acid[13] from surface and subsurface groundwater,[9,19,20] thereby improving water/sewage purification treatments.

Adsorption, from an engineering point of view, refers to the diffusion[3] of metal into the core of the CS bead.

---

* Corresponding author. Tel.: +1 801 581 8854; fax: +1 801 581 8433; e-mail: grant@chem.utah.edu

Table 1. Metal amount before and after chelation to CS and CSGA, respectively

Metal cation	Conc. (mmol/L)	Salt used	Mass of wet beads (g)	End pH		Concentration of metal cations		
				CS	CSGA	AA before adsorption (ppm)	ICP after adsorption (ppm)	
							CS	CSGA
Cr^{6+}	5.77	$K_2Cr_2O_7$	30.0	7.30	7.34	300.0	46.25	12.81
Mn^{2+}	5.46	$MnSO_4 \cdot H_2O$	30.0	7.38	7.48	300.0	10.70	8.60
Fe^{2+}	5.37	$FeSO_4 \cdot 7H_2O$	30.0	4.19	4.19	299.9	42.03	19.70
Co^{2+}	5.09	$CoSO_4$	30.0	6.45	6.96	300.0	17.52	7.60
Ni^{2+}	5.11	$NiCl_2 \cdot 6H_2O$	30.0	6.63	6.69	300.0	99.48	37.16
Cu^{2+}	4.72	$CuSO_4$	16.6	6.04	6.56	299.7	232.41	146.06
Zn^{2+}	4.59	$ZnSO_4 \cdot 7H_2O$	30.0	6.54	6.73	300.1	53.79	13.43

From a microscopic view, however, adsorption involves a physical or chemical interaction between the metal ion and the polymer. In this study, metal complexation is investigated using mainly solid state NMR spectroscopy and X-ray powder diffraction analysis (XRPD) supported by other solid-phase analysis.

Little is known about metals binding to the nitrogen of the C-2 amines in CS and of the imines in CSGA. Metals have been proven to favor –CH and –CH$_2$ from the aldehyde linker of GA and –CH$_3$ from partially deacetylated CS ($78 \pm 3\%$), which is supported by XRPD and CP/MAS data in this study. Metals seem to favor interaction with the amorphous region of CS.[9] The amorphous region is known to have hydrophilic pockets containing water, nitrogen sites, and hydroxyl alcohols from both C-6 and the glucosamine monomeric ring structure. Voth and co-workers[21] described in detail that excess protons in Nafion®, which is a sulfonated tetrafluorethylene copolymer (synthetic polymer),[22] contribute to solvation and delocalization within, forming a hydrophilic pocket with a high degree of inter- and intra-polymer hydrogen bonding. CS is similar to Nafion®[23] except CS exists naturally with similar ionic properties to Nafion® and can be used as proton-exchange membrane in fuel cells[23] due to many hydrophilic carriers[24] within the polymer. In this chapter, a series of metal ions complexed with CS and its cross-linked derivatives are investigated, showing that these amorphous regions interact with different metals in different ways, depending upon the oxidation state of the metal.

2. Materials

Chitosan (CS) with a molecular weight of 94 ± 4 kDa, a bead size of a 3.8 mm diameter and degree of acetylation of $22 \pm 3\%$ was processed from chitin extracted from Cape lobster shells. Glutaraldehyde cross-linked chitosan (CSGA) gel beads have a water content of $95 \pm 0.1\%$ (w/w) and a 22% degree of cross-linking. The metal–polymer complexes (Cr, Mn, Fe, Co, Ni, Cu, and Zn) of both CS and CSGA, in the form of gel beads, were provided by Vaal University of Technology, South Africa. The nitrogen mole fraction content of a glucosamine polymer is 8.69% for 0% acetylation[1] and that of a fully acetylated N-acetylglucosamine polymer is 6.89%.[1] Nitrogen content for our samples can then be calculated as 8.294% for 22% acetylation.

The chitin extraction procedure has been described in detail by Muzzarelli[25] in the *Chitin Handbook*, and the detailed cross-linking procedure has been described by Hsien and Rorrer[26] in 1997. The equilibrium end pH values, referring to the pH at equilibrium between the adsorbed metal ions and that in the solution of all samples, were kept constant using 0.1 M HNO$_3$/NaOH solution and are specified in Table 1. Metal uptake was done at 25 ± 0.5 °C. The wet beads as received were crushed into a paste, dried at 1000 rpm at a low temperature in a speed-vacuum setup for 4 h, and finally was crushed further into very fine powder for all physical measurements.[27]

3. Methods

3.1. Metal cationic concentration measurement

Metal ion concentrations in the various reagents were measured using a Varian SpectrAA-10 with a resolution error of $\pm 5\%$ at Vaal University of Technology, South Africa before absorption. The amount of metal incorporated into the metal–polymer complexes was measured with ICP using a Perkin–Elmer Optima 3100XL ICP-OES at the Department of Hematology, School of Medicine, University of Utah Health Sciences Center, Salt Lake City, Utah.

3.2. Solid-state nuclear magnetic resonance spectroscopy (SS NMR)

High-resolution ^{13}C MAS spectra for all samples were obtained at 14.1 T on a Varian® Infinity 600 Plus spectrometer using a 4-mm PENCIL™ dual resonance probe. The sample size is approximately 100 mg spinning at 10 kHz. All experiments used the CP technique

with the Hartmann–Hahn match established in hexamethylbenzene (HMB), rather than the polyglycan peaks with their broad line widths. The ^{13}C shifts were referenced to the methyl resonance of HMB at 17.35 ppm, and the magic angle was optimized by observing the highest intensity of this resonance.

The FIREMAT technique applies five π pulses synchronized with magic-angle turning (MAT) and simultaneously allows determination of all chemical shift tensors in a molecule. Since FIREMAT employs the CP technique at the first part of the pulse sequence,[28–31] accurate use of contact time, T_1 relaxation time and an exact Hartmann–Hahn match[32] are essential to the experiment. Careful calibrations of the *rf* pulses as well as optimal *rf* amplitudes for both proton and carbon channels are important. Contact time is sample dependent. Detailed experimental setup for FIREMAT in this study has been discussed previously.[33–35]

3.3. TIGER (technique for importing greater evolution resolution) processing[36]

TIGER is a convolution processing technique similar to Fourier transform, which helps transform 2D FID with higher resolution in a shorter acquisition time on the evolution dimension (second dimension). TIGER takes the isotropic carbon chemical shift from the evolution dimension, generates a high-speed MAS 1D guide spectrum, three principal tensor values and one unique sideband pattern per isotropic shift from the experimental dimension (first dimension). These sideband patterns are fitted using the banded matrix approach[37] and mark the exact fingerprint in chemical shift anisotropy per carbon.[38,39]

3.4. X-ray powder diffraction (XRPD) analyses

All XRPD patterns were collected using a Bruker AXS DiffracPlus D8 Advance diffractometer with a Cu anode at 1.540629 Å Cu Kα radiation (Kα1 = 1.54060 Å, Kα2 = 1.54439 Å, and Kβ = 1.39222 Å) using a Göbel mirror operated at 40 kV with intensity of 40 mA. Samples of 275 mg were spread evenly on an open plastic tray, and its surface was carefully flattened. The tray was placed on a fixed standard sample stage on one axis of the diffractometer. A monochromatic beam of radiation is generated from the Cu source and impinges on the sample. The incident beam and the detector on the mobile reflected arm are tilted by an angle θ, which is called the θ/θ configuration. A 0.1 mm detector slit was placed in both incident and diffracted beams coupled with a 0.6 mm divergent slit and a 1 mm anti-scattering slit. Data points were collected every 2 s and measured as a function of scattering angle, 2θ, in the range from 5–85° using a step size of 0.02° in the scan angle. The corresponding spacing (*d*) between scattering planes is simultaneously converted and is recorded along with the 2θ value at each data point.

3.5. Electron spin resonance (ESR) spectroscopy

Paramagnetic properties of all samples were screened with 30 scans at 9.756 GHz (X band) and at 34.8 GHz (Q band) using a Bruker EMX ER-082 spectrometer. The signal was referenced to the center field of 3473.785 G under a magnetic strength of 9.746 GHz of zero phase, receiver gain of 5.03×10^3, conversion of 40.96 ms, time constant of 5.12 ms and sweep time of 41.943 s. The magnetic field (B) for the ESR was calibrated using diphenylpicrylhydrazyl (DPPH) positioned close to the sample as a field marker (*g*) of 2.002320.

3.6. Far-Fourier transform infrared (far-FTIR) spectroscopy

Far-FTIR spectroscopy provides a mean of measuring the low frequency vibrational motions that are useful in characterizing many organometallic and inorganic molecules. The results of such measurements often allow the chemical nature and molecular structure of an organometallic complex to be identified. Far-FTIR absorption focuses mainly on the 50–650 cm^{-1} region and is particularly useful for probing the vibrational frequencies between heavy atoms that have weak bonds, such as the low frequency metal–ligand vibrations of the polymeric complexes. CSs complexed with Cu and with Ni have the highest metal cation-to-polymer ratio, and were measured with far-FTIR spectroscopy in this study. The powder specimen was ground with Nujol oil in an agate mortar to a uniform paste and then placed onto polyethylene (PE) film. The sample paste was then observed using a Bruker Tensor 37 Far-FTIR spectrometer with 16 scans in the mid-to-far IR range.

3.7. Theoretical calculations

The molecular structures were set up using Gauss-View®.[40] Molecular geometry optimization and atomic charge calculations were performed using the GAUSSIAN 03®[41] MP2 (Møller–Plesset perturbation theory)[42] approach proposed by Pople and co-workers[41,43–45] and using the d95** basis set.

4. Results

4.1. Metal interaction in the –CH, –CH$_2$, and –CH$_3$ shift regions

Sixteen CP/MAS spectra were recorded for uncomplexed chitosan and glutaraldehyde cross-linked
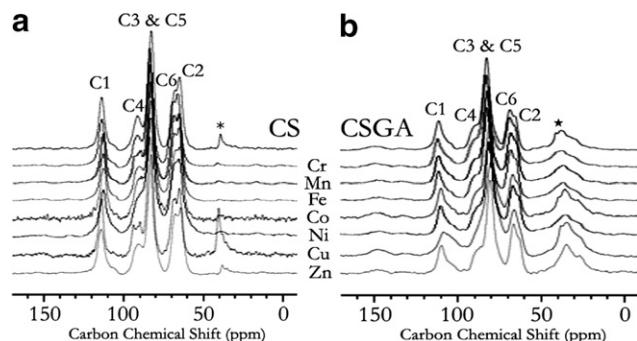
Figure 1. CP/MAS spectra of metal complexed with (a) CS (left) and (b) CSGA (right). All transition metal ions are in the order of Cr to Zn (top to bottom). * indicates the residual CH_3 from chitin that remains after deacetylation. ★ indicates the CH and/or CH_2 from glutaraldehyde (GA) cross-linkage.

chitosan as well as these metal–polymer complexes. All sixteen CP/MAS spectra display five distinct peaks with an extra broad region around the carbon chemical shift of 20 ppm. For CS, this broad region (indicated by * in Fig. 1) represents the methyl carbon on the acetyl group of chitin remaining in the 22% acetylated portion as impurities in CS. Only CS, CS complexed with Cu, and CS complexed with Zn (CSCu and CSZn) have a distinct peak in this region. The other CS–metal (CSM) complexes apparently interact differently with the polymers, thereby affecting the peak intensity of this methyl region. For CSGA, a broad region (indicated by * in Fig. 1) is much wider than that of CS (~17–22 ppm). This is the region in which the –CH and –CH_2 units of the glutaraldehyde linkage are found. CSGA alone and CSGA complexed with Co, Cu, and Zn (CSGACo, CSGACu, and CSGAZn, respectively) appear to have higher intensity in this region, most likely indicating a lower occupancy of metal ions in the cross-link region. Hence, the lower intensity of this broad region indicates greater metal binding in the vicinity of the cross-link.

4.2. Two torsion angles in two sideband patterns of one isotropic shift

The glycosidic bonding from anomeric C-1 of one glucosamine ring to C-4 of the next glucosamine ring has two conformational degrees of freedom, which are specified by the two torsion angles ϕ and ψ through the glycosidic bond illustrated in Figure 2. Normally, these two angles are of intermediate or average form when the polymer is at equilibrium. From the FIREMAT sideband patterns, the presence of Mn and Cu significantly affects the β,β-conformation in an inhomogeneous way, leading to two sideband patterns with one isotropic chemical shift entry from C-4 shown in Figure 2. These two sideband patterns of C-4 represent two torsion angles at the glycosidic linkage that involves C-1, O, and C-4 in the
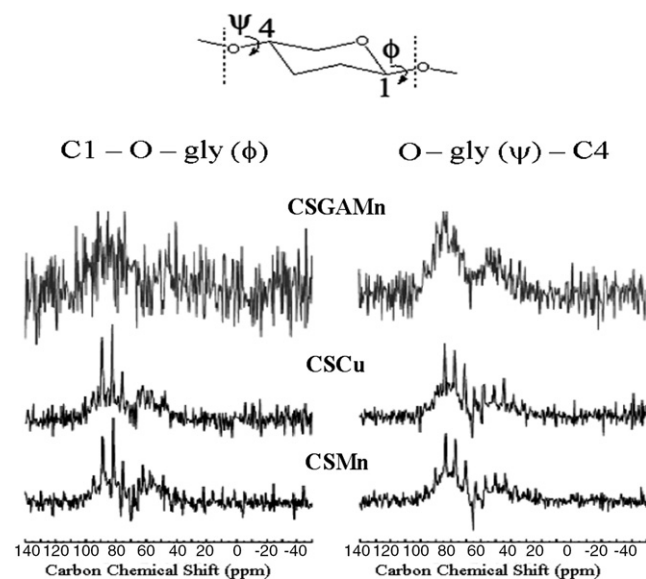
Figure 2. Two distinct sideband patterns generated from FIREMAT data with one single isotropic input of C-4 indicate that Mn and Cu separately interact with the two torsion angles.

glycosidic bond, namely C-1–O–Gly (labeled as ϕ) and O–Gly–C-4 (labeled as ψ).[46] The sideband patterns affected by these two separate torsion angles at the glycosidic linkage in the metal–polymer complexes are seen in SS NMR spectrum for the first time.

The specific sidebands observed for each chemical shift in the metal–polymer complexes all have similar patterns, which indicate that the metal perturbation in both polymers is small compared with the large average size of the polymers (94 ± 4 kDa), and no Knight shifts are observed. The anisotropy for the methyl residue of chitin in the CSGAFe complex is extremely broad, which overlaps and covers the sideband patterns for C-2 in CSGAFe. CSNi seems to have coupling effects with all sideband patterns except the merged peak of C-3 and C-5. CSGACu has a similar effect and is likely due to the higher metal-to-polymer ratio of Cu and Ni compared with the other metal complexes.

4.3. Observation of metal interaction using XRPD

Figure 3 shows a comparison between the XRPD patterns of CS and CSGA. The signal at the scanned angle $2\theta = 29.26°$ is a very homogeneous line, which represents a crystalline component in the polymeric lattice. The sharp peaks at the larger scanned angles from $2\theta = 33–85°$ represent a crystalline region in the polymer and remain the same in both CS and CSGA. The two broad peaks in the ranges of $2\theta = 9–13°$ and $10–23°$ come from the amorphous regions[3] that were previously ignored in earlier literature. By comparing CS and CSGA, the only significant chemical difference between the two polymers is an amino–imino conversion at C-2
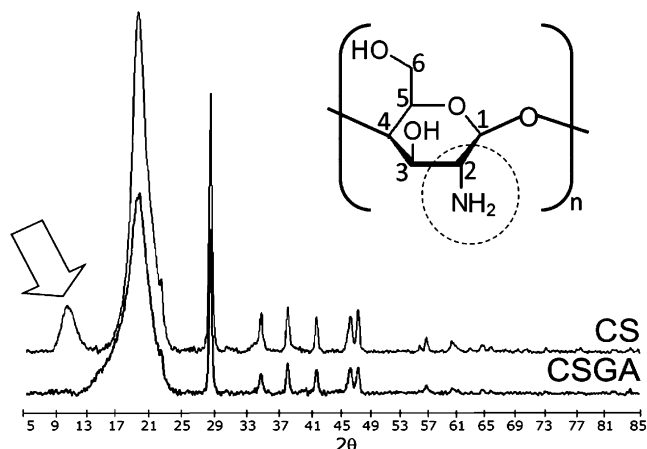
Figure 3. A comparison in the XRPD patterns of CS and CSGA measured using Bruker AXS DiffracPlus D8 Advance diffractometer scanned from $2\theta = 5$–$85°$. Inset is the chemical structure of CS with the amino region circled at C-2. The arrow points to the broad region in CS, which corresponds to the missing region in CSGA.
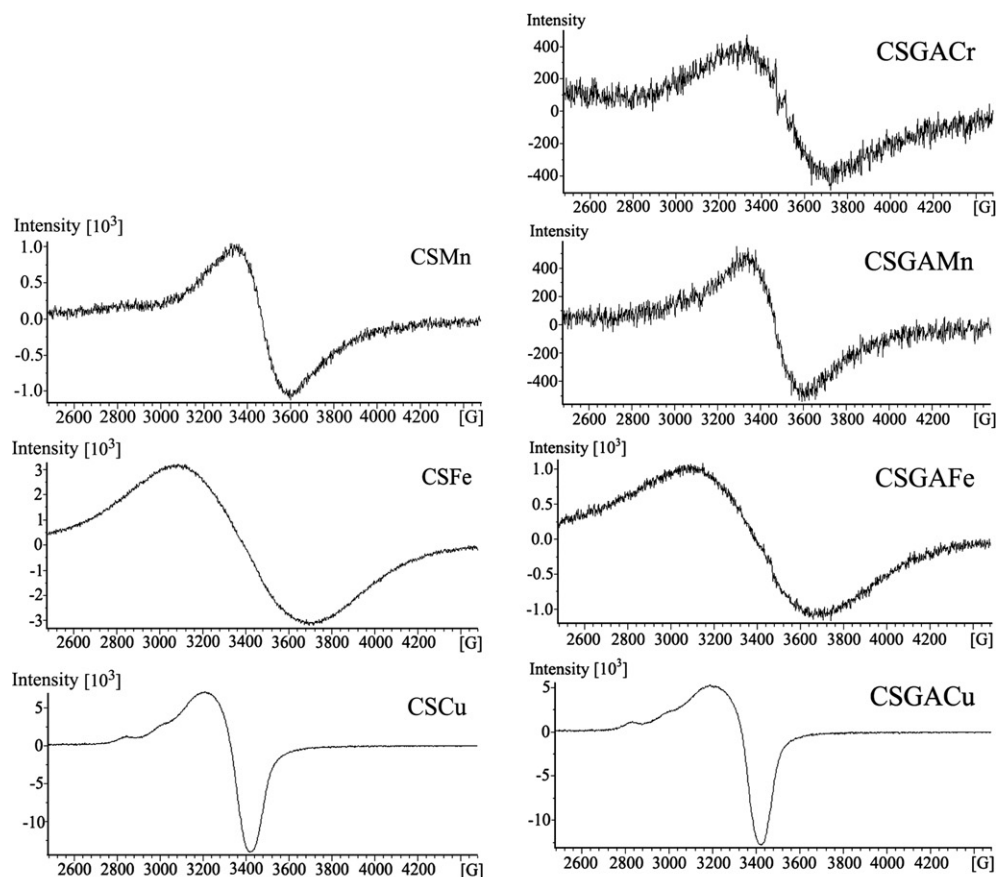

Figure 4. XRPD patterns for CSM complexes. Inset is the chemical structure of CS with the amino region at circled C-2. The arrow points to the corresponding broad diffraction peak in CS.

with a doubling of the molecular size of CSGA compared to CS. The first broad region found in the XRPD pattern for CS disappeared in the XRPD pattern for CSGA, indicating that this feature in the diffraction pattern of CS is associated with disorder in the C-2 amino group. This broad region is absent in the CSGA diffraction scan because the amino group has been converted to an imino group in the cross-linked polyglycans. Some nitrogen sites must remain as amino groups in the cross-linked polymer, however, because the cross-linker concentration is low. The XRPD patterns also suggested that there is a high possibility of a change in oxidation state during the chelation process. In order to further investigate this nitrogen region around $2\theta = 9$–$13°$ and the amorphous region between 10–$23°$, all other peaks are scaled to the intensity of the peak at the scanned angle $2\theta = 29.26°$ for the relative comparison of all metal–polymer complexes.

Metals (M) seem to interact with the amino group of CS, particularly in disordered portions of the polymer. This is evidenced by changes in the $2\theta = 9$–$13°$ peak as a function of complexed metal ion, shown in Figure 4. The varying intensity of the amino peak in the different metal complexes with CS shows that different metals bind to the CS in different ways. In particular, Co and Zn preserve the disordered amino peak, while other metal ions reduce the intensity of this feature significantly when complexation occurs. Similar observations were found in the CSGAM complexes shown in Figure 5. The second broad region from $2\theta = 10$–$23°$, which corresponds to the hydrophilic pockets in the polymers, exhibits different intensity depending on which metals are complexed. The reduced intensity of the feature in the metal–polymer complexes indicates that the metal ions are complexed in the hydrophilic pocket.
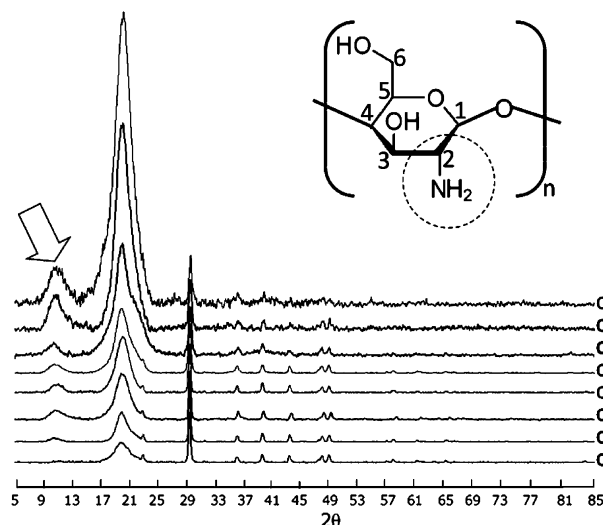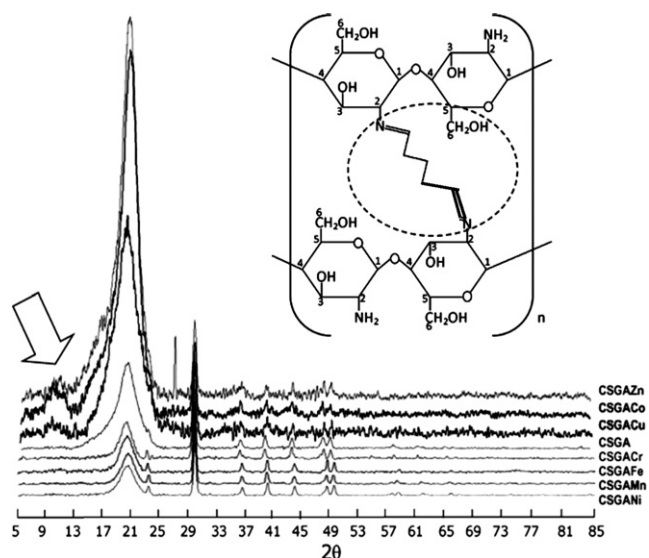
Figure 5. XRPD patterns for CSGAM complexes. Inset is the chemical structure of CSGA with the imino linker at C-2 circled. The arrow points to the corresponding amino region of CS, which absent in CSGA.

4.4. ESR observations

ESR spectroscopy is a direct measurement of electron spin when there are unpaired electrons within a chemical structure. It provides a way to investigate the electronic spin state and oxidation state of metal adsorbed in both CS and CSGA. Figure 6 shows ESR signals for Mn, Fe, and Cu complexed with both CS and CSGA. In addition, Cr complexed with CSGA also has an ESR signal, but there is no ESR signal observed with Cr complexed with CS. The complexes involving Co, Ni, and Zn exhibited no ESR signal.

Figure 6. Mn, Fe, and Cu complexed with both CS (left) and CSGA (right) showed strong ESR signals, whereas only CSGACr showed an ESR signal. Oxidation states and outer shell electrons are summarized: M = metal; d = d-shell electrons; − indicates no ESR signal; + indicates ESR signal observed.

M	CS			CSGA		
	Oxidation State	Outer Shell electrons	ESR Signal	Oxidation State	Outer Shell electrons	ESR Signal
Cr	?	?	−	3+	d^3	+
Mn	2+	d^5	+	2+	d^5	+
Fe	3+	d^5	+	3+	d^5	+
Co	2+	d^6	−	2+	d^6	−
Ni	2+	d^8	−	2+	d^8	−
Cu	2+	d^9	+	2+	d^9	+
Zn	2+	d^{10}	−	2+	d^{10}	−

The strong ESR signal of CSGACr complex indicates an oxidation state of Cr^{3+} due to the unpaired d^3 electronic configuration, whereas the ESR non-responsive CSCr complex could implicate several conditions within the CSCr complex. The absence of an ESR signal for CSCr cannot be interpreted without a definitive measurement. There may be two forms of stable chromium found in the environment: Cr^{3+} and Cr^{6+}. Since the reagent for Cr chelation was potassium dichromate ($K_2Cr_2O_7$), there is a high possibility that the dichromate ions remain in CS after the metal uptake process. Masri[18] in 1978 reported on the matter of chromium uptake, in which both CS and CSGA are capable of attracting metal cations, hydrogen ions and metal anions such as dichromate, depending on the pH value during complexation. Binding cations and hydrogen ions involve binding the associated anions at the same time, whereas the latter involve protonation of the poly-

mer as a result of being a positive charge carrier. Secondly, the unpaired electron from Cr^{3+} may couple with the free radical within the CS polymeric chain, which in turn shields the shields the paramagnetic property of the Cr^{3+}, giving no ESR signal. Several earlier studies have reported that CS and cross-linked CS have the ability to remove Cr^{6+} from waste water.[9,47] Cr^{6+} is a strong oxidizing agent, which has the capability of forming a sandwich moiety within the polymer, is considerable.[48]

Strong ESR signals with both CS and CSGA complexed with Mn and Fe indicate that both Mn and Fe should have the d^5 electronic configuration, whereas the oxidation state for Mn should be in its divalent state, and Fe should be in its trivalent state.[48]

Cobalt and nickel are relatively unreactive and are stable in a divalent ionic spin state with $S = 0$. It is very difficult to obtain ESR signals of these metals.[48]

Copper has a single s electron outside the filled 3d shell with formal stoichiometry in the +1 oxidation state.[48] The d^9 configuration makes Cu^{2+} subject to Jahn–Teller distortions[49–51] if placed in a cubic, octahedral or tetrahedral system. This asymmetric stereochemistry contributes to the paramagnetic/magnetic effect of the sample properties, giving strong ESR signals with both CS and CSGA.

Zinc, however, with a filled d shell may be considered as a Group IIB element instead of a transition metal ion.[48] Divalent Zn ions have an $S = 1$ spin state that gives very insignificant ESR signals.

Co, Cu, and Zn chelated with both CS and CSGA systems seem to have a more octahedral or severely distorted geometry[48] as compared with the individual polymeric framework, whereas the geometries of Cr, Mn, Fe, and Ni are more likely different than those of Co, Cu, and Zn within the hydrophilic pockets of the polymeric chains.

4.5. Amino region confirmed with far-FTIR

The metal ions seem to interact with the amorphous regions where the amine groups are located, as supported by the XRPD patterns and confirmed by far-FTIR spectrometry. The strongest adsorption samples were the CSCu and CSNi, which were examined and compared with CS using the far-FTIR technique. CSNi shows IR signals in the amine region at about 400 cm^{-1}, indicating that the metal ions interact and bond to the amine groups within the hydrophilic pockets of the polymers.

4.6. Theoretical calculations

Nitrogen sites were evaluated theoretically (Table 2) with an amino carrier (–NH$_2$), and an imino carrier (=NH–) bonded with simple alkyl carbons to an extended alkyl chain. Both the amino and the imino models carry negative charges (−0.580 and −0.178,

respectively), but the imino carrier was less negative than the amino carrier. As the imino carrier bonded with a longer alkyl chain, the change on the nitrogen becomes slightly negative (−0.254) compared with the imino carrier alone. Interestingly, as the length of the alkyl chain of the imino linker grows longer, the charge again becomes less negative, indicating a shift of the negative charge originally located on the nitrogen migrating toward the alkyl linker. This phenomenon is similar to benzene or other compounds containing conjugate double bonding in which there is a resonance effect from the π-electrons in benzene and other conjugated compounds.

Another theoretical model was evaluated by placing a proton between a hydroxyl group of an alcohol and an amine/imine attachment at C-2 on the glucosamine ring shown in Figure 7. The positions of the alcohol and the amine/imine were held constant, while the position of the proton was varied. From the comparison between the starting distance to the final distance of the proton between –OH and –N in the amine/imine, respectively, provides a strong proof that the amine forms stronger hydrogen bonding than the imine. From the plot, the end distance between an amine to a proton is more stable, indicating that the hydrogen bonding that forms in the amino model shows a stronger hydrogen interaction. The end distance between an imine to a proton, however, shows a looser or weaker interaction, indicating the presence of an electron transfer to and-fro between the proton and the imine, leaving a less stable structure, which is also consistent with the transfer of resonance π-electrons in the previous theoretical model on the nitrogen sites.
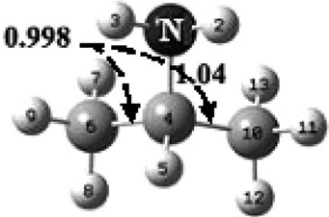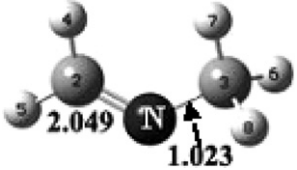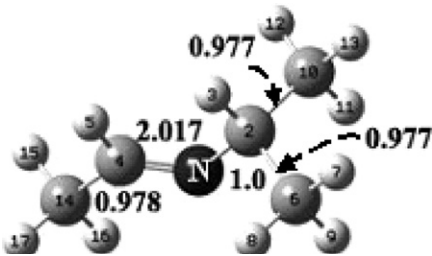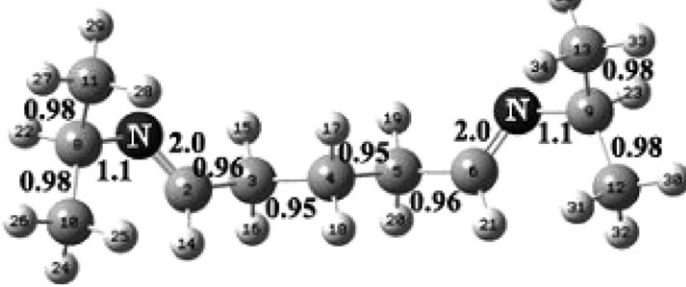
The role of electrons from nitrogen on the amine/imine or from oxygen were also considered in a previous study.[14] Lone pairs of electrons have the ability to bind to a proton or complex with a metal ion through electron-pair sharing. A nitrogen site would have a stronger ability to donate the lone pair of electrons in sharing with a metal ion than an oxygen site since oxygen has a stronger attraction of the lone pair of electrons to its nucleus.[14]

With the differences in valency and oxidation state of different metal ions, more stereochemical restraint by hindrance and packing could occur due to the slightly positive imine linker and the competitive amino sites, leading to fewer metal ions chelated into the CSGA chains, which is not what prior studies predicted.

5. Discussion

CS exhibits a helical coil structure as discussed in earlier studies,[52] and behaves structurally like single-stranded DNA containing intra-hydrogen bonding due to the presence of many hydroxyl groups and amine sites in

Table 2. Theoretical models of charge calculation on nitrogen for amine, imine, and imino linker

Theoretical models for amine/imine/imino linker	Mulliken charges on N
	−0.580
	−0.178
	−0.254
	−0.246

Starting Distance	Final Distance	
	Imine	Amine
0.8	2.0166	1.9107
0.9	2.0026	1.9117
1.0	1.9797	1.9112
1.1	1.9334	1.9118
1.2	1.9348	1.9117
1.3	1.9406	1.9117
1.4	1.9480	1.9109
1.5	1.9386	1.9120
1.6	1.9380	1.9119
1.7	1.9457	1.9115
1.8	1.9395	1.9112
1.9	1.9347	1.9114
2.0	1.9393	1.9123
2.1	1.9465	1.9113
Average	1.9527	1.9115
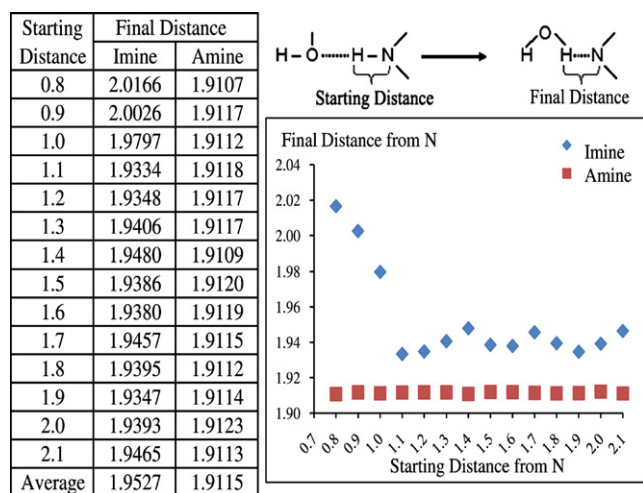
Figure 7. A theoretical comparison between the distance of an imine or an amine attachment at C-2 to a hydroxyl group.

the polymeric chain. This characteristic creates a unique hydrophilic pocket, which gives the long- and short-range structural disorder found in the helical coil itself and contributes to the amorphous nature of CS.

The cross-linking process with glutaraldehyde (GA) doubles the molecular size of CS with the addition of extra GA linkages. The carbonyl groups on both ends of the GA bond with the nitrogen atoms from the amino groups on each CS forming an imino linkage (Schiff base). This stabilizes the CS structure and would increase the metal ion binding surface area as well as the number of metal ion binding sites for CS, contrary to the results of this study.

The percentage of cross-linking in CSGA was reported as non-related to metal absorption by Monteiro and Airoldi.[53] Increasing the degree of cross-linking decreases the flexibility of CS chains, but the metal uptake ability remains the same. A previous cross-linking study

with CS focused only on the increase in surface area forming a single-stranded helical coil of CS, while the iminoaldehyde replaced the amine at C-2 only superficially in one CS chain rather than in conjunction with two or more CS chains at a time.[10] Ideally, this superficial replacement of an amine with an iminoaldehyde should increase the surface area for CS if CS stayed in a single-stranded coiled mode. The iminoaldehyde group contributes to the bulky part of the CS, which would not allow the CS to coil and would reduce the flexibility of the CS chain itself. The single, coiled cross-linked module may not be acceptable due to steric hindrance from the bulky glutaraldehyde linker to the neighboring alcohols.

Capitani et al.[15] report a cross-linked CS with 1,1,2,3-tetramethoxypropane (TMP). The alkyl linker in the TMP cross-link is approximately half of the size of that in glutaraldehyde. Two CS chains with one TMP module joined in an antiparallel fashion was proposed for the CSTMP cross-linked model. The antiparallel structure seems to be necessary to maintain the β-(1→4)-linked glycosidic conformation between the glucosamine units and the axial position for C-2 and C-5 per glucosamine ring to allow homogeneous spectral lines in SS NMR.

Due to the diverse behavior between the amino and imino nitrogen, not all the amino sites are replaced with imines. Transition metal ions are also structurally restrained by their metal spin/oxidation states, which only allow certain metal chelation complexes in the polymers. Other attractions from the neighboring alcohols from the polymers also allow inter- and intra-hydrogen bonding with the metal ions, leading to more structural constraints and steric hindrance between each helical turn. These restrictions on the metal-chelation moiety include a hydrogen-bonding limit of one metal ion binding to many glucosamine units.

The shapes of the sideband patterns serve as chemical fingerprints and represent the structural interactions within the complex. Nitrogen coupling to proton(s) and metal cationic interaction may appear as broad and noisy patterns, particularly for C-2. Sidebands for C-2, C-4, and C-6 seem to have stronger metal coupling effects than the other sidebands for both metal complexes. This interesting feature confirms that C-2 and C-5 all occupy axial positions to the same plane in a β,β-polymeric conformation.

These sideband patterns can also be explained with the structural constraint due to the twist-and-turn of the CS chain itself. Clark and Smith[54] in 1936 completed the first X-ray fiber pattern of CS in its acidic salt form, and it was not interpreted until 1997.[55] Ogawa et al.[52] in 2004 summarized the structures of different acidic salts of CS. The CS coil was described as taking four glucosamine units in order to complete a helical turn. This tetrasaccharide makes a long fiber repeat of 40.8 Å. A fiber pattern has been unobserved for CS alone in the past. A helical-coil CS model is proposed in Figure 8, which shows the twisting CS chain in a helical string and describes how metal (M) ion absorption interacts with neighboring alcohols forming inter- and intra-hydrogen bonding within the CS helical chain.

Through sideband patterns, only C-2, C-4, and C-6 are mainly affected by metal-ion intercalation into the CS with only the Ni complex having a C-1 contribution. Metal ions could only be found at the center core of the helical coil interacting with the nitrogen sites from the amino groups at C-2 of the opposite glucosamine units and leaving the other two nitrogen sites of the neighboring glucosamine units free to the outer surface of the helical turn.

Position C-6 on the glucosamine unit contributes as an electron donor by donating an H^+ from the hydroxyl group of the alcohol, while position C-6 of the opposite glucosamine unit contributes by donating the hydroxyl group from the alcohol of the polymer. Consequently, a water molecule is released, and a temporary bonding with the metal ion forms at the center of the helical turn. Depending on the valency and the oxidation state of the metal ion, there could be loose bonding between each helix as well. This adds a great deal of complexity to the long- and short-range disorders between helical coils of CSM complexes. In addition, the helical turns of these CSM complexes are packed more tightly than the others, leaving broad anisotropy and acentricity of the sidebands with huge amorphous regions in the XRPD patterns. The likelihood of metal ions penetrating every helical unit, or even every other unit, would depend on the valency of each metal ion, which means that some metal ions would bind in only one helical loop, whereas others may correlate with several helical loops. This same reason explains why some complexes manifest C-2, C-4, and/or C-6 influence, but some only have C-4 and/or C-6 influence. Positions C-1 and C-4, on the other hand, are related to the glycosidic linkage suppressed or restrained by the metal bonding with the neighboring nitrogen and oxygen sites.

Sideband patterns also suggest some features for the manner of metal chelation in CSGA. A 2C1L proposed model with one imino linker sandwiched between two-chitosan chains is presented in Figure 9. Two antiparallel CS chains may cross-link with GA forming CSGA by forming an imino bond between the nitrogen from the amino group of CS and the two end carbonyl group from the GA. Cross-linking needs to be present on the exterior of the helical coils to coexist with the antiparallel CS chains twisting together to form a double-stranded helical structure. The metal would be loosely bound on the surface of the CSGA chains, thereby increasing the binding ability of the CSGA as compared to CS. Metal ions, however, were proven by the above
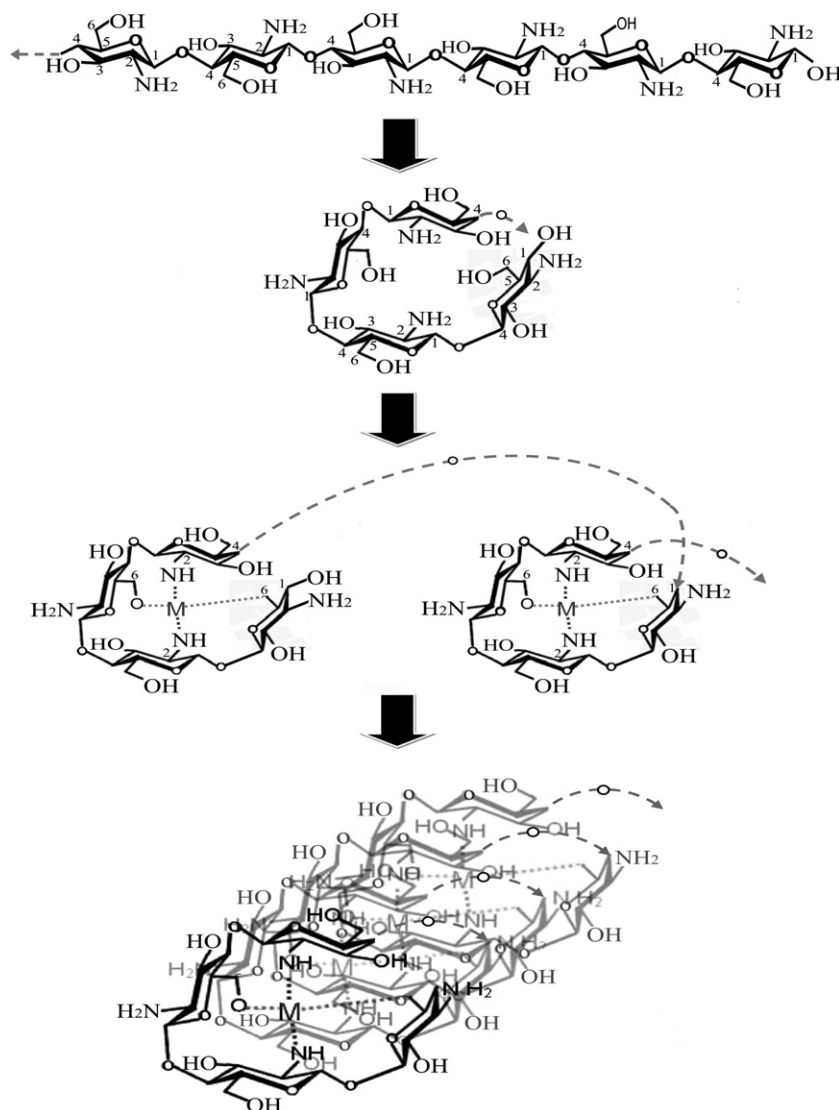
Figure 8. The twisting-and-turning behavior of a single CS chain in a helical spiral with metal cations interacts at center of the helical turn. Carbon schema are designated only for the first two glucosamine units and the glycosidic bond.

models for the first time to be more likely absorbed within the polymeric chains rather than adsorbed superficially as expected in the past.

Structural disorder or imperfection appears to be simply a distortion of the crystal lattice, which amounts to a variation of interplanar spacing (d) within or between domains due to the nature of the powder samples. Dislocation of the crystal lattice could be expected to contribute to broad linewidths in XRPD due to the average separation involved between adjacent planes.[56] The alternative positions for atoms or groups of atoms in this distorted crystal spread out the electron density from the ideal-ordered positions leading to an increase of static disorder and hence reduce diffracted intensities especially at higher scanned angles ($2\theta = 33$–$85°$). Badly disordered structures give diffraction patterns in which the intensities fall off rapidly at higher angles. Mobile

structures with more degrees of structural freedom within the crystal lattice, such as crystals that have long alkyl chains, non-planar ring structures, loose ions of high symmetry without strong intermolecular interactions, and small molecules unconstrained by hydrogen bonding, also create more disorder in the crystal lattice.

Twinned crystals within the metal–polymer complexes would contribute to another type of unusual diffraction, such as one that contains two or more orientations or mirror images of the same structure within the crystal lattice, but still maintains a well-defined unit cell relationship. A twinned diffraction pattern is a result of superposition of many individual diffracted patterns per crystal moiety. Diffraction patterns of a polymer, for instance, may even have reflections that coincide at various measured lattice points.[57]
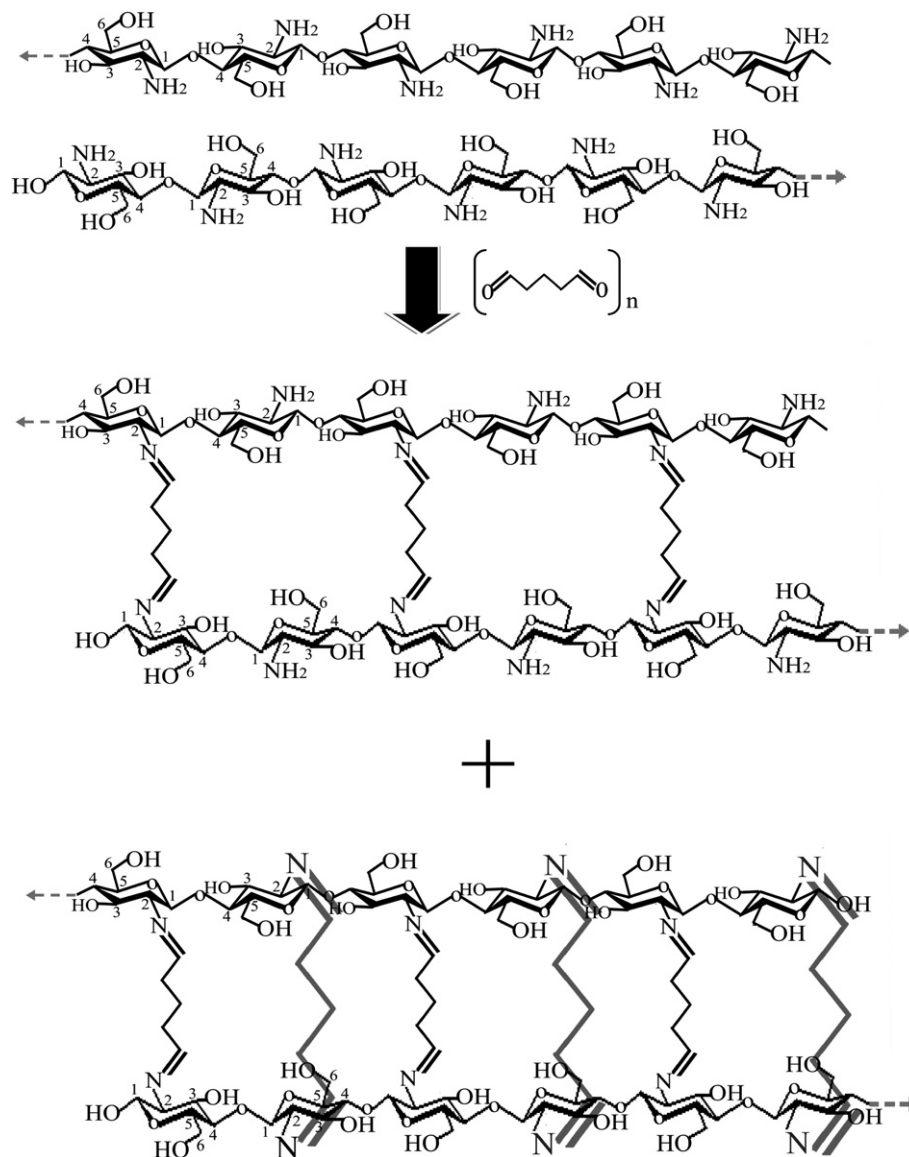
Figure 9. Two CS chains cross-linking with GA forming CSGA in the condition that the amino group from CS becomes an imino group by bonding with the carbonyl groups at both ends of GA. Carbon schema are designated only for the first two glucosamine units and the glycosidic bond.

ICP-OES results in Table 1 also showed that CSGA seems to adsorb smaller amounts of metal ions in ppm compared with those chelated with CS itself, suggesting that all of the metal ions are not binding on the exterior surface of the double-stranded CSGA chains. Also, not all amino sites have changed to imino sites by cross-linking. Cross-linkages may interfere with the internal structure of the helical coil, allowing some of these nitrogen sites on the exterior to coordinate with the metal link as well. The ICP-OES data are also consistent with the theoretical metal–polymer ratio.

A Mössbauer study by Bhatia and Ravi[8] on the CSFe complexes confirm that iron exists in the high-spin ferric state consisting of five unpaired electrons, which is consistent to our ESR result. However, Bhatia and Ravi also claimed that Fe^{3+} occupied a penta- or a hexa-coor-

dination, which may not be true. Their proposed scheme showed that Fe^{3+} would bond with two nitrogen sites, two alcohols, and two hydrogens from the polymer of unknown sources. Our observation from SS NMR confirmed the previously stated unknown source as the free hydroxyl group from the alcohol at C-6 in the glucosamine unit. Instead of being a free planar or rhombic structure, we proposed an octahedral structure with two nitrogen sites and two alcohol groups from the opposite glucosamine units in the same square plane with two extra alcohol hydroxyl groups from C-6 above and below the square plane.

Hydrogen bonding reported in previous literature, especially between $O(3) \cdots O(5)$ intramolecularly[52] and $CH_2OH(6)$ intermolecularly[2] was supported by the proposed proton affinity theoretical model by placing a
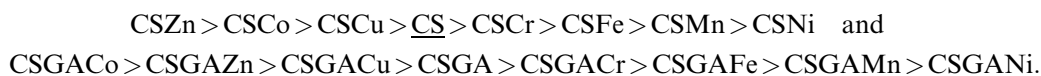
proton between a hydroxyl group of an alcohol and an amine/imine nitrogen.

A Schiff's base (imine) is known to be relatively unstable and exists only in a temporary structural status. Transfer of π-electrons from an imino nitrogen to the aldehyde linker and resonance within the glutaraldehyde cross-link are seen in the theoretical model. The pH also contributes a great amount of the protonation of nitrogen.[10] At neutral or alkaline pH, the nitrogen at C-2 in CS favors the form of $-NH_2$, which the nitrogen sites are unprotonated and uptake of metal ions is favored.[9] In an acidic environment, the nitrogen at C-2 in CS favors $-NH_3^+$. The protonated nitrogen sites carry positive charges, which significantly decrease the nucleophilicity of nitrogen but stabilize the Schiff's base and increase the ability to attract anions. Iron, which binds at a lower pH, is the only exception.

6. Conclusions

The theoretical data and the ICP-OES data for metal uptake in CSGA are consistent. This decrease in the amount of the metal uptake shown in ICP-OES data for the CSGA compared with CS alone, the increase of linewidth for the amorphous region from the XRPD patterns and the broadened spectral lines from the SS NMR spectra suggest that CSGA may be in a form of two CS chains in the antiparallel fashion connected with two imino nitrogens of C-2 to the antiparallel CS chains. The aldehyde groups of GA are displaced by the nitrogens forming a Schiff's base. The surface area of CSGA relative to CS increases, but cross-linking increases the competition of metal-binding nitrogen sites, which decreases the metal uptake in CSGA. We proposed that the cross-linked structure is likely a double-stranded helical coil of two CS units sandwiched with one aldehyde linker from GA.

The effect from the spin state and oxidation state of the metal ligands within the metal–polymer complexes with the observed amorphous region in XRPD is confirmed further by ESR spectrometry. The scaled peak intensity of the amorphous region from the XRPD patterns appeared in a progressively decreasing order:[27]

$$CSZn > CSCo > CSCu > \underline{CS} > CSCr > CSFe > CSMn > CSNi \quad \text{and}$$
$$CSGACo > CSGAZn > CSGACu > \underline{CSGA} > CSGACr > CSGAFe > CSGAMn > CSGANi.$$

References

1. Sherpherd, R.; Reader, S.; Falshaw, A. *Glycoconjugate J.* **1997**, *14*, 535–542.
2. Harish Prashanth, K. V.; Kittur, F. S.; Tharanathan, R. N. *Carbohydr. Res.* **2002**, *50*, 27–33.
3. Piron, E.; Accominotti, M.; Domard, A. *Langmuir* **1997**, *13*, 1653–1658.
4. Guzman, J.; Saucedo, I.; Revilla, J.; Navarro, R.; Guibal, E. *Int. J. Biol. Macromol.* **2003**, *33*, 57–65.
5. Mukoma, P.; Jooste, B. R.; Vosloo, H. C. M. *J. Power Sources* **2004**, *136*, 16–23.
6. Cervera, M. F.; Heinamaki, J.; Rasanen, M.; Maunu, S. L.; Karjalainen, M.; Acosta, O. M. N.; Colarte, A. I.; Yliruusi, J. *Carbohydr. Polym.* **2004**, *58*, 401–408.
7. Guibal, E.; Milot, C.; Eterradossi, O.; Gauffier, C.; Domard, A. *Int. J. Biol. Macromol.* **1999**, *24*, 49–59.
8. Bhatia, S. C.; Ravi, N. *Biomacromolecules* **2000**, *1*, 413–417.
9. Schmuhl, R.; Krieg, H. M.; Keizer, K. *Water SA* **2001**, *27*.
10. Wang, T.; Turhan, M.; Gunasekaran, S. *Polym. Int.* **2004**, *53*, 911–918.
11. Ho, Y.-S. *Brazilian J. Chem. Eng.* **2005**, *22*, 319–322.
12. Burke, A.; Yilmaz, E.; Hasirci, N.; Yilmaz, O. *J. Appl. Polym. Sci.* **2001**, *84*, 1185–1192.
13. Gotoh, T.; Matsushima, K.; Kikuchi, K.-I. *Chemosphere* **2004**, *55*, 135–140.
14. Jin, L.; Bai, R. *Langmuir* **2002**, *18*, 9765–9770.
15. Capitani, D.; Crescenzi, V.; De Angelis, A. A.; Segre, A. L. *Macromolecules* **2001**, *34*, 4136–4144.
16. Gotoh, T.; Matsushima, K.; Kikuchi, K.-I. *Chemosphere* **2004**, *55*, 57–64.
17. Loretz, B.; Bernkop-Schnurch, A. *AAPS (E)* **2006**, *8*, 756–764.
18. Masri, M. S.; Randall, V. G.; Pittman, A. G. *Polym. Prepr. (Am. Chem. Soc., Div. Polym. Chem.)* **1978**, *19*, 483–488.
19. Guibal, E.; Jansson-Charrier, M.; Saucedo, I.; Le Cloirec, P. *Langmuir* **1995**, *11*, 591–598.
20. No, H. K.; Meyers, S. P. *J. Agric. Food Chem.* **1989**, *37*, 580–583.
21. Petersen, M. K.; Wang, F.; Blake, N. P.; Metiu, H.; Voth, G. A. *J. Phys. Chem. B* **2005**, *109*, 3727–3730.
22. Caja, J.; Czerwinski, A.; Rubinson, K. A.; Helneman, W. R.,; Mark, H. B., Jr. *Anal. Chem.* **1980**, *52*, 1010–1013.
23. Wan, Y.; Peppley, B.; Creber, K. A. M.; Bui, V. T.; Halliop, E. *J. Power Sources* **2006**, *162*, 105–113.
24. Wang, H.; Fang, Y.-E.; Yan, Y. *J. Mater. Chem.* **2001**, *11*, 1374–1377.
25. Muzzarelli, R. A. A.; Peter, M. G. Chitin Handbook; Atec: Grottammare, It, 1997.

26. Hsien, T. Y.; Rorrer, G. L. *Ind. Eng. Chem. Res.* **1997**, *36*, 3631–3638.

27. Webster, A.; Grant, D. M.; Osifo, P. O.; Neomagus, H. W. J. P. *A Systemic X-ray Powder Diffraction Study of Seven Selected Metal Cations Chelated into Chitosan and Chitosan Cross-linked with Glutaraldehyde*; Bruker Axs: Madison, Wis, 2006, pp 1–8.

28. Pines, A.; Gibby, M. G.; Waugh, J. S. *J. Chem. Phys.* **1972**, *56*, 1776–1777.

29. Pines, A.; Gibby, M. G.; Waugh, J. S. *J. Chem. Phys.* **1973**, *59*, 569–590.

30. Pausak, S.; Pines, A.; Waugh, J. S. *J. Chem. Phys.* **1973**, *59*, 591–595.

31. Harris, R. K. Cross-polarization. In *Solid State NMR*; Pitman Books Ltd, 1983; pp 149–151.

32. Hartmann, S. R.; Hahn, E. L. *Phys. Rev.* **1962**, *128*, 2042–2053.

33. Alderman, D. W.; McGeorge, G.; Hu, J. Z.; Pugmire, R. J.; Grant, D. M. *Mol. Phys.* **1998**, *95*, 1113–1126.

34. Grant, D. M. In *Five-π Pulse Magic Angle Turning Spectra of Solids*; Wiley: Chichester, 2002; Vol. 9, pp 73–91.

35. Webster, A.; Osifo, P. O.; Neomagus, H. W. J. P.; Grant, D. M. *Solid State Nucl. Magn. Res.* **2006**, *30*, 150–161.

36. McGeorge, G. H.; Jian, Z.; Mayne, C. L.; Alderman, D. W.; Pugmire, R. J.; Grant, D. M. *J. Magn. Reson.* **1997**, *129*, 134–144.

37. Alderman, D. W.; Solum, M. S.; Grant, D. M. *J. Chem. Phys.* **1986**, *84*, 3717–3725.

38. Antzutkin, O. N.; Shekar, S. C.; Levitt, M. H. *J. Magn. Reson.* **1995**, *115*, 7–19.

39. Antzutkin, O. N.; Lee, Y. K.; Levitt, M. H. *J. Magn. Reson.* **1998**, *135*, 144–155.

40. Dennington, R., II; Keith, T.; Millam, J.; Eppinnett, K.; Hovell, W. L.; Gilliland, R. GaussView, 3.09; Semichem: Shawnee Mission, KS, 2003.

41. Pople, J. A. GAUSSIAN 03, C.01; Gaussian: Wallingford CT, 2004.

42. Møller, C.; Plesset, M. S. *Phys. Rev.* **1934**, *46*, 618–622.

43. Pople, J. A.; Krishnan, R.; Schlegel, H. B.; Binkley, J. S. *Int. J. Quant. Chem. Symp.* **1978**, *14*, 545–560.

44. Frisch, M. J.; Head-Gordon, M.; Pople, J. A. *Chem. Phys. Lett.* **1990**, *166*, 275–288.

45. Handy, N. C.; Schaefer, H. F., III. *J. Chem. Phys.* **1984**, *81*, 5031–5033.

46. Saito, H.; Tabeta, R.; Ogawa, K. *Macromolecules* **1987**, *20*, 2424–2430.

47. Nomanbhay, S. M.; Palanisamy, K. *Electronic J. Biotechnol.* **2005**, *8*, 43–53.

48. Cotton, F. A.; Wilkinson, G. The Elements of the 1st Transition Series. In *Advanced Inorganic Chemistry*; John Wiley & Sons: New York, 1962; 29, pp 661–664, 681–683, 687, 694–695, 707–708, 711–714, 719–720, 723–758; 470–480.

49. Brunker, T. J.; Green, J. C.; O'Hare, D. *Inorg. Chem.* **2003**, *42*, 4366–4381.

50. Soltis, S. M.; Strouse, C. E. *J. Am. Chem. Soc.* **1988**, *110*, 2824–2829.

51. Crabtree, R. H. Stereochemistry of Dissociative Substitution. In *The Organometallic Chemistry of the Transition Metals*; John Wiley & Sons: New York, 2001; pp 97–98.

52. Ogawa, K.; Yui, T.; Okuyama, K. *Foods Food Ingred. J. Jpn.* **2004**, 209.

53. Monteiro, O. A. C.; Airoldi, C. *Int. J. Biol. Macromol.* **1999**, *26*, 119–128.

54. Clark, G. L.; Smith, A. F. *J. Phys. Chem.* **1937**, *40*, 863–879.

55. Okuyama, K.; Noguchi, K.; Miyazawa, R.; Yui, T.; Ogawa, K. *Macromolecules* **1997**, *30*, 5849–5855.

56. Langford, J. I.; Louer, D. *Rep. Prog. Phys.* **1996**, *59*, 131–234.

57. Clegg, W. Crystal Structure Analysis: Principles and Practice. *International Union of Crystallography*; Oxford University Press: Chester, UK, 2001, pp 185–190.